

RESEARCH ARTICLE

10.1029/2018JC014233

Special Section:

Forum for Arctic Modeling and Observational Synthesis (FAMOS) 2: Beaufort Gyre phenomenon

Key Points:

- Beaufort Gyre mooring measurements of velocity and temperature are analyzed for subinertial signal
- Observations are consistent with topographic Rossby waves propagating on sloping seafloor
- Topographic Rossby waves play a role in Beaufort Gyre stabilization

Correspondence to:

B. Zhao,
bowen.zhao@yale.edu

Citation:

Zhao, B., & Timmermans, M.-L. (2018). Topographic Rossby waves in the Arctic Ocean's Beaufort Gyre. *Journal of Geophysical Research: Oceans*, 123. <https://doi.org/10.1029/2018JC014233>

Received 1 JUN 2018

Accepted 24 AUG 2018

Accepted article online 29 AUG 2018

Topographic Rossby Waves in the Arctic Ocean's Beaufort Gyre

Bowen Zhao¹  and Mary-Louise Timmermans¹ 

¹Department of Geology & Geophysics, Yale University, New Haven, CT, USA

Abstract A 5-year long time series of temperature and horizontal velocity in the Arctic Ocean's Beaufort Gyre is analyzed with the aim of understanding the mechanism driving the observed variability on timescales of tens of days (i.e., subinertial). We employ a coherency/phase analysis on the temperature and horizontal velocity signals, which indicates that subinertial temperature variations arise from vertical excursions of the water column that are driven by horizontal motions across the sloping seafloor. The vertical displacements of the water column (recorded by the temperature signal) show a bottom-intensified signature (i.e., decay toward the surface), while horizontal velocity anomalies are approximately barotropic below the main halocline. We show that the different characteristics in vertical and horizontal velocities are consistent with topographic Rossby wave theory in the limit of weak vertical decay. In essence, a linearly decaying vertical velocity profile implies that the whole water column is stretched/squashed uniformly with depth when water moves horizontally across the bottom slope. Thus, for the uniform stratification of the deep water column, the response in the relative vorticity field (ensuring conservation of potential vorticity) is also uniform with depth, leading to the observed barotropic horizontal velocity changes. The prevalent topographic Rossby wave activity is discussed in context with Beaufort Gyre spin-up, dissipation, and stabilization.

Plain Language Summary A 5-year long time series of temperature and velocity in the Arctic Ocean's Beaufort Gyre is analyzed to understand the source of water motions that occur with periods of tens of days. We find that vertical water motions are driven by horizontal flows across the sloping seafloor. The vertical motions are strongest near the seafloor. On the other hand, horizontal motions in the deep Beaufort Gyre are approximately uniform with depth. We show that these characteristics are consistent with topographic Rossby waves, which are waves associated with water moving horizontally across a seafloor slope. The prevalent topographic Rossby wave activity is discussed in context with energetics and stabilization of the changing Beaufort Gyre.

1. Introduction

The anticyclonic Beaufort Gyre, centered over the Arctic's Canada Basin, is a dominant feature of the Arctic Ocean circulation. The intensity and energetics of the Beaufort Gyre govern heat and freshwater storage and transport, influencing sea ice and Arctic and global climate (e.g., Proshutinsky et al., 2009). The response of the gyre to changes in wind forcing involves the excitation of Rossby waves; although the polar regions have only weak β effect (and hence weak planetary Rossby waves), seafloor topography in the Canada Basin gives rise to topographic Rossby waves (TRWs; e.g., Luneva et al., 2012; Timmermans et al., 2010; Yang et al., 2016). As such, TRWs are an essential element of Beaufort Gyre spin-up, geostrophic adjustment, and dissipation, although they have been little studied in observations. This study analyzes Beaufort Gyre mooring measurements to understand the presence and dynamics of TRWs.

The Beaufort Gyre is characterized by a strong halocline stratification and, below around 300-m depth, a deeper more weakly stratified ocean (Figures 1 and 2). The temperature stratification is dominated by the warm core of the Atlantic Water Layer centered around 450-m depth (Figure 1). Deeper than this, there are subtle yet rather complex water mass layers, the evolution of which have been examined in a number of studies (e.g., Carmack et al., 2012; Dosser & Timmermans, 2018; Timmermans & Garrett, 2006; Timmermans et al., 2003, 2005; Woodgate et al., 2007). Below the core of the warm Atlantic Water Layer, potential temperature decreases with depth to a minimum at about 2,400 m. Deeper than this temperature minimum, temperature increases through a transition layer toward the top of a well-mixed bottom water layer extending from ~2,750-m depth to the ocean bottom, ~3,500 m (Figure 3a). The transition layer temperature profile has

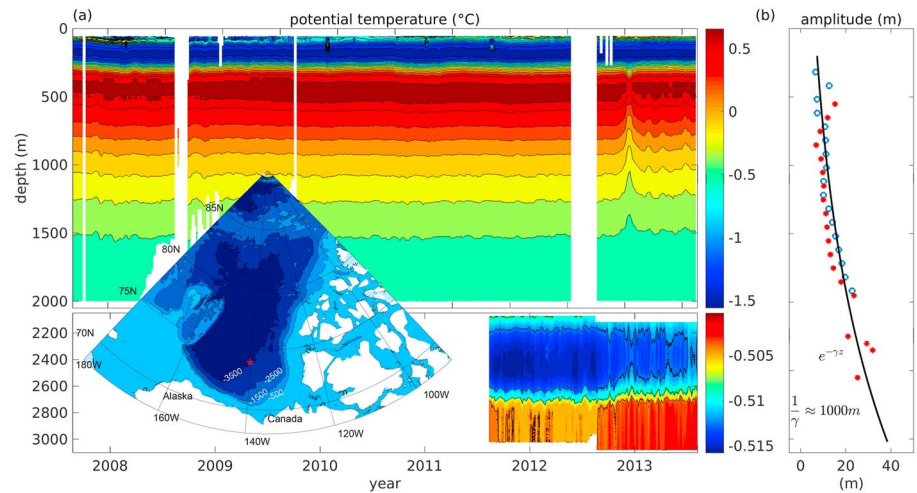


Figure 1. (a) Depth-time series (6 years) of potential temperature θ ; the mean over 5 days is shown. Measurements are from Beaufort Gyre Observing System Mooring D (located at the red star shown on the inset map) at 74°N , 140°W , in the vicinity of a weak bottom slope. Note that the upper 2,000 m and that below are from the shallow and deep McLane Moored Profilers, respectively, and are shown with different color scales. (b) Standard deviation of isopycnal displacements (blue circles) and isotherm displacements (red stars) at selected depths (see text). The black curve is the exponential fit to the profile of isopycnal displacements, with a vertical decay length of $\sim 1,000$ m. Data after 23 August 2012 are excluded from this analysis (see text).

a staircase structure (possibly a double-diffusive staircase), a region which has been shown to exhibit both inertial and subinertial motions (Timmermans et al., 2007).

Analyzing a yearlong mooring record of deep potential temperature measurements in the Beaufort Gyre, Timmermans et al. (2010) characterized the dominant subinertial frequency to be around 50 days; they found that coherent vertical water column excursions (inferred from the temperature signal) exist through the water column with displacement amplitudes decaying approximately exponentially toward the surface. This is

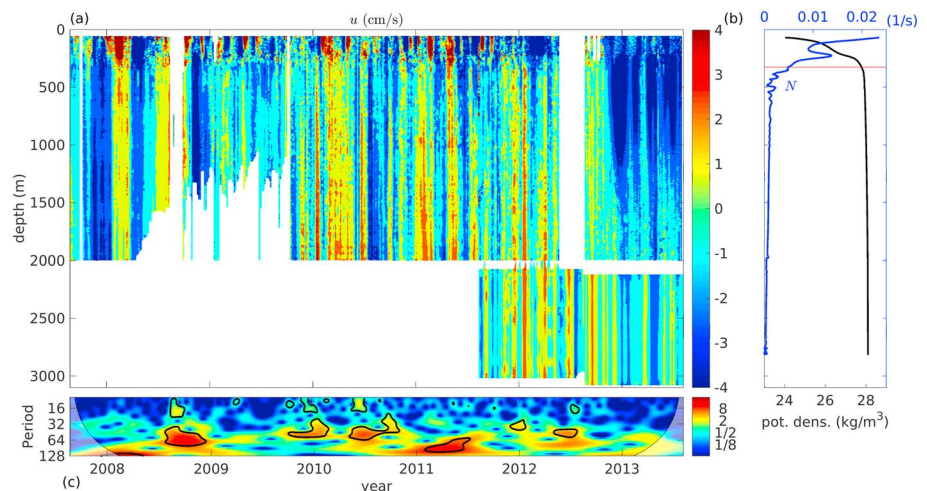


Figure 2. (a) Depth-time series (6 years) of east-west u speed; the mean over 5 days is shown. The north-south speed (not shown) shows similar characteristics. Shallow and deep McLane Moored Profiler data are shown with the same color scale (cf. Figure 1a). (b) The mean profile of potential density anomaly referenced to the surface (black) and the mean buoyancy frequency ($N^2 = -\frac{g}{\rho_0} \frac{\partial \rho}{\partial z}$, blue). Potential density is computed by averaging depths of a given isopycnal for all density profiles before 23 August 2012. The horizontal red line denotes the depth (~ 300 m) where N becomes weak and approximately uniform with depth. (c) The wavelet transform of vertically averaged u below ~ 300 m. The white shaded cone of influence indicates the maximum period of useful information at that particular time. Periods longer than this are subject to edge effects. The black contour indicates the 5% significance level against red noise. Note the concentration of power between ~ 30 and ~ 100 days.

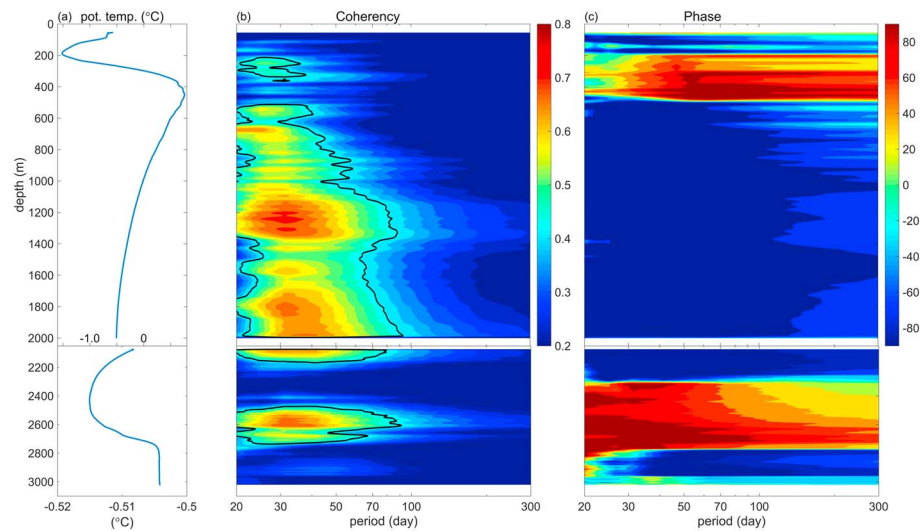


Figure 3. (a) Time-averaged potential temperature θ as a function of depth. Note that the temperature scale is different for the upper (top x axis) and lower (bottom x axis) portions. (b) Coherency and (c) phase between vertically averaged $u-v$ and θ over all depths. The black contour in (b) denotes the 95% confidence level for coherency, ~ 0.44 . To ensure consistency between the shallow and deep calculations, coherency/phase results are presented from a yearlong record for both the shallow and deep Mooring (2011–2012). Extending this for the entire shallow mooring time series yields similar results.

typical of TRWs (e.g., Rhines, 1970; Shu et al., 2016; Thompson & Luyten, 1976), which arise from conservation of potential vorticity applying to topographically induced water column stretching/squashing. Cross-slope flows give rise to water column stretching (squashing), which induces anomalous positive (negative) relative vorticity to ensure conservation of potential vorticity. The anomalous relative vorticity field induces further cross-slope motions nearby: The perturbations thus propagate, with shallow water on the right in the Northern Hemisphere, as TRWs in much the same way as planetary Rossby waves propagate westward under the β effect.

Adopting reasonable estimates of the ocean bottom slope and stratification structure, Timmermans et al. (2010) derived a TRW dispersion relation for the Canada Basin and showed consistency with the ~ 50 -day subinertial period characterizing the temperature observations. Here we analyze a longer time series of moored measurements, including horizontal velocity information, to further understand these motions. One dominant feature that our analysis aims to explain is the observation that subinertial horizontal motion is approximately uniform in depth below the strongly stratified halocline (i.e., in the water column deeper than ~ 300 m). Approximately barotropic horizontal flow would appear to be inconsistent with the bottom-intensified TRW inferred from potential temperature measurements and described by Timmermans et al. (2010). In this paper, we resolve this apparent discrepancy by pointing out that the Beaufort Gyre stratification below the halocline is sufficiently small that the weak decay limit of the TRW solution applies. For context, the deep Beaufort Gyre stratification is more than an order of magnitude smaller than stratification of North Atlantic regions previously studied for their TRW activity (e.g., Johns & Watts, 1986; Pickart & Watts, 1990; Thompson & Luyten, 1976; Zhao et al., 2018).

This paper is organized as follows. Section 2 describes the mooring measurements. In section 3, we present results from a spectral analysis to demonstrate the relationship between subinertial potential temperature variations and velocity variations. This allows us to proceed in section 4 by exploring the dynamics of the motions in order to reconcile the apparent discrepancy between the barotropic horizontal motion and the bottom-intensified vertical motion. Having demonstrated that these energetic features that dominate deep water column dynamics are TRWs, we summarize and discuss the implications of our conclusions to Beaufort Gyre energetics and stabilization in section 5.

2. Measurements

The data examined here consist of mooring measurements of horizontal velocity, temperature, salinity, and pressure from McLane Moored Profilers (MMPs) deployed at a single location in the Canada

Basin (Figure 1a, inset). The mooring is *Mooring D* of the set of Beaufort Gyre Observing System (BGOS, <http://www.whoi.edu/beaufortgyre/>) moorings (see details in ; Proshutinsky et al., 2009; Timmermans et al., 2010). Horizontal velocity (u , v), potential temperature (θ), and salinity (S) profiles are measured from about 55- to $\sim 2,000$ -m depth by an MMP profiling the upper and intermediate water column (over a period spanning 24 August 2007 to 2 August 2013) and from $\sim 2,073$ - to $\sim 3,021$ -m depth by an MMP profiling the deep water column (from 14 August 2011 to 8 August 2013). We will refer to the upper profiler as the *shallow* MMP and the lower as the *deep* MMP. Profiles are returned every ~ 6 hr and then ~ 48 hr (shallow MMP) and every ~ 8 hr and then ~ 11 hr (deep MMP). We analyze measurements processed to a vertical resolution of ~ 2 m (shallow MMP) or ~ 1 m (deep MMP; see Proshutinsky et al., 2009, for further details). Finally, we note that the BGOS includes shallow MMP Mooring D data after August 2013, although a deep MMP was not deployed on the mooring after this time.

Potential temperature measurements show the clear signal of the warm Atlantic Water Layer, the deep transition to a warm homogeneous bottom layer, and water column heaving (Figure 1a). Horizontal velocity measurements over 2007–2012 show deviations to higher velocity that appear to be approximately uniform over the water column below ~ 300 m (Figure 2a). Time series of velocity components at selected depth levels below ~ 300 m show a high degree of similarity in subinertial variability (i.e., variations at one depth match variations at all other depths with no change in magnitude or phase; not shown). In particular, the 2011–2012 deep MMP measurements of u and v (east-west and north-south velocities, respectively) clearly match the shallow MMP measurements (Figure 2a). Motions in the top ~ 300 m appear in general to be distinct from those below, suggesting different sources of variations dominating above versus below the halocline; energetic mesoscale eddies are ubiquitous in the Beaufort Gyre halocline (e.g., Zhao et al., 2016). In the discussion that follows, we will only refer to motions below the halocline (deeper than around 300 m).

Notably, after late 2012 the water column below the halocline and shallower than 2,000 m is dominated by the influence of what appear to be cyclonic eddies centered around the core of the Atlantic Water Layer (~ 400 m, Figures 1a and 2a). The energetic cyclonic eddies are not a prominent feature in the earlier part of the record (2007–2012), and it appears that there has been some transition in water column dynamics in 2013 compared to 2007–2012; for this reason, we choose to limit the focus of this study to 2007–2012 unless otherwise noted. Understanding the temporal transition in dynamics will likely provide important understanding with respect to the Beaufort Gyre region but is outside the scope of this study.

3. Interpretation of Subinertial Potential Temperature Variations

The 5-year long time series (2007–2012) shallower than 2,000 m and the 2011–2012 deep time series ($>2,100$ -m depth) show the persistence of subinertial variations in θ on several tens of days over the water column (Figure 1a). A wavelet analysis of both potential temperature (not shown) and horizontal velocity (vertically averaged below ~ 300 m, Figure 2c) reveals subinertial motions of period around 50 days, consistent with Timmermans et al. (2010). On the assumption of no mixing and no intrusions of new water masses (having differing temperature and salinity properties but the same density), we may convert θ variations to vertical displacements (i.e., water column heaving). To do this, we take the profile at the start of the record to be the reference temperature profile and estimate the difference (in depth) between selected isotherms in all subsequent profiles and the reference depth of the chosen isotherm. For a given isotherm, the root mean square displacement is computed over the full time series. Isopycnal displacements derived in the same way closely correspond to water column displacements estimated from isotherm variability (Figure 1b). This correspondence between isotherm and isopycnal displacements lends support to our assumptions that there are no intrusions of new water masses nor mixing, and it is reasonable to assume that the observed variations are due to vertical water column heaving (see also Timmermans et al., 2010). Note that the horizontal translation of the water column past the mooring may also give rise to isotherm/isopycnal variations; however this can be ruled out given the weak horizontal gradients and weak horizontal advection in the vicinity (see Timmermans et al., 2010); we verify this assumption shortly. We estimate the vertical exponential decay scale of isopycnal/isotherm displacements (excluding the eddy-dominated 2013 segment) to be about 1,000 m, similar to the estimate of Timmermans et al. (2010) that was based on a 1-year record (Figure 1b). Next we show how the subinertial potential temperature variations (Figure 1) are consistent with lateral advection over a sloping bottom driving a vertical velocity w (water column heaving). Note that the amplitude of w variations should be proportional to the amplitude of isotherm (isopycnal) displacement variations and hence should also be bottom intensified.

Mooring D is located in the vicinity of sloping topography, and it is therefore reasonable to speculate that the vertical motions result from cross-slope horizontal motions. The bottom slope (∇h) at Mooring D shoals toward the southeast, which yields a condition for the vertical velocity at the seafloor, $w_0 = -\frac{\partial h}{\partial x}u - \frac{\partial h}{\partial y}v \propto u - \alpha v$, where α is the ratio $|\frac{\partial h}{\partial y}|/|\frac{\partial h}{\partial x}|$ (x and y are east-west and north-south coordinates, respectively). An examination of International Bathymetric Chart of the Arctic Ocean bathymetry (Jakobsson et al., 2012, with a resolution of approximately 1 km in the horizontal) indicates $\alpha \approx 1$ at Mooring D, and hereafter, we set $\alpha = 1$.

It proves insightful to examine the correspondence between measured horizontal velocity and temperature variations. The coherency between $u-v$ (vertically averaged below 300 m) and θ at various depths is found to be high and statistically significant in a substantial region of the frequency-depth domain (Figure 3b). The high coherency holds in the frequency domain starting around periods of ~ 20 days and extends to periods of ~ 100 days. We note the lack of coherency in three depth ranges: around 500-m depth, around 2,400-m depth, and below 2,800-m depth. These depths are all associated with vanishing vertical temperature gradient $\partial\theta/\partial z$ (Figure 3a). Around 500 and 2,400 m, $\partial\theta/\partial z$ vanishes as θ approaches extrema, the warm core of the Atlantic Water Layer and the deep temperature minimum, respectively. Deeper than 2,800 m, $\partial\theta/\partial z$ vanishes in the homogeneous bottom layer. In regions of nonnegligible $\partial\theta/\partial z$, we expect temperature variations (resulting from vertical water column heaving) to be coherent with $u-v$ for vertical advection resulting from cross-slope horizontal motions. This further implies that a sign reversal of $\partial\theta/\partial z$ should lead to a reverse in sign of the phase between $u-v$ and θ . Indeed, the phase below the temperature maximum at ~ 500 m is around -90° , reversing to around 90° below the temperature minimum at 2,400 m (Figure 3c). The absolute value of 90° of the phase is consistent with temperature variations being driven by vertical velocity. As mentioned previously, the temperature signal could conceivably arise from horizontal advection of a horizontal temperature gradient $\partial\theta/\partial x$. However, the phase reversal above and below temperature extrema is not consistent with this; similarly, horizontal advection should not yield zero coherency around vanishing $\partial\theta/\partial z$. Having demonstrated the importance of cross-slope motions in causing subinertial θ variations, we next show how they are consistent with TRWs.

4. Source of the Variability: A TRW

The fact that the vertical velocity w derives from cross-slope horizontal motions may appear to be inconsistent with w possessing a different vertical decay scale from that of the horizontal flow u and v . Here we explain the relationship between horizontal and vertical flow in the context of a TRW.

To understand the source of subinertial variability, we begin by reviewing the findings of Timmermans et al. (2010) who start with the Boussinesq quasi-geostrophic potential vorticity (QGPV) equation in the limit of subinertial motion (i.e., $\omega \ll f$, where ω is the frequency of the motion and f is the Coriolis parameter) and with negligible β effect:

$$f_0^2 \frac{\partial^2 w}{\partial z^2} + N_0^2 \left[\frac{\partial^2 w}{\partial x^2} + \frac{\partial^2 w}{\partial y^2} \right] = 0, \quad (1)$$

where f_0 is the (constant) Coriolis parameter and $N_0 \approx 2f_0 = 2.8 \times 10^{-4} \text{ s}^{-1}$ is the constant buoyancy frequency above the bottom mixed layer. The buoyancy frequency varies only weakly below the halocline, which allows an approximation of constant N_0 above the homogeneous bottom layer (Figure 2b). Assuming (1) has a separable solution with plane wave in the horizontal, that is, $w = \hat{w}(z)\exp[i(kx + ly - \omega t)]$, yields

$$\frac{d^2 \hat{w}}{dz^2} = \left[\frac{K_H N_0}{f_0} \right]^2 \hat{w} = \gamma^2 \hat{w}, \quad (2)$$

where $K_H = \sqrt{k^2 + l^2}$ is the horizontal wave number and $\gamma = K_H N_0 / f_0$ is the vertical decay scale. Hereafter, hatted variables indicate wave amplitudes. As explained by Timmermans et al. (2010), the homogeneous bottom layer effectively shifts the ocean bottom ($z = -H$) to the top of the bottom homogeneous layer ($z = -H_T$); the Taylor-Proudman theorem stipulates that the velocity at the top of the homogeneous layer is equal to the velocity at the seafloor. In particular, $w(z = -H_T) = w(z = -H) = w_0 = -\frac{\partial h}{\partial x}u - \frac{\partial h}{\partial y}v$. The bounded solution above the homogeneous bottom layer ($z \geq -H_T$) is

$$\hat{w} = w_0 \exp[-\gamma(z + H_T)]. \quad (3)$$

Here the top boundary of the domain ($z = 0$) is taken to be at the 300-m level. However, note that (3) implies that $\hat{w}(z = 0) = w_0 \exp(-\gamma H_T)$, which is necessarily small. This requires that $\gamma H_T \gg 1$. That is, the decay

is strong and the important possibility of weak decay is excluded. Combining the hydrostatic and buoyancy equations yields

$$\frac{1}{\rho_0} \frac{\partial^2 p}{\partial z \partial t} = -N_0^2 w. \quad (4)$$

This implies that pressure p (and therefore also u and v) would undergo exponential decay in the vertical with the same decay scale as w . This is inconsistent with observations, which indicate an effectively barotropic horizontal flow over the domain of interest. We argue that the apparent inconsistency results from the condition adopted by Timmermans et al. (2010) to ensure boundedness of the flow far from the ocean bottom. This condition imposes a strong vertical decay and hence cannot yield the observed barotropic structure.

We argue that a rigid-lid boundary condition is likely a more suitable top boundary condition given the Beaufort Gyre's strong halocline stratification (see Veronis, 1981). Requiring that $w(z = 0) = 0$ and $w(z = -H_T) = w_0$ yields the solution to (2):

$$\hat{w} = -\frac{w_0}{\sinh(\gamma H_T)} \sinh(\gamma z). \quad (5)$$

Correspondingly,

$$\hat{p} = \frac{i}{\omega} \frac{\rho_0 N_0^2 w_0}{\gamma \sinh(\gamma H_T)} \cosh(\gamma z), \quad (6)$$

where the appearance of imaginary unit i indicates the $\pi/2$ phase difference between the pressure perturbation p and the vertical velocity perturbation w . In the limit of weak decay (i.e., $\gamma H_T \ll 1$),

$$\hat{w} \approx -\frac{w_0 \gamma}{\sinh(\gamma H_T)} z \quad (7)$$

$$\hat{p} \approx p_0 = \frac{i}{\omega} \frac{\rho_0 N_0^2 w_0}{\gamma \sinh(\gamma H_T)}. \quad (8)$$

This solution yields linear vertical decay of w above the bottom, while the pressure and horizontal velocity remain approximately constant with depth, agreeing well with the measurements. Note that although we employed an exponential fit to the vertical profile of isopycnal displacements (Figure 1b), the profile may be equally well described by a linear fit due to the weak damping. Then the observed weak decay, $\gamma H_T \ll 1$ or $K_H H_T \ll f_0 / N_0 \approx 1/2$, with $H_T \approx 2,500$ m, yields

$$K_H \ll 2 \times 10^{-4} \text{ m}^{-1} \quad \text{or} \quad \lambda_H \gg 30 \text{ km}, \quad (9)$$

where λ_H is horizontal wavelength. Note that the weakly decaying TRW solution derived here yields a longer λ_H than that estimated by Timmermans et al. (2010) who found ~ 12 km based on (3) with $\gamma \approx 0.001 \text{ m}^{-1}$ for the exponentially decaying TRW solution.

The physical scenario may be easily understood in terms of conservation of potential vorticity and taking the water column to be composed of a series of stacked thin layers. A linearly decaying \hat{w} implies that each layer simultaneously squashes or stretches by the same amount when the water column moves up or down the slope, respectively. To conserve potential vorticity, the relative vorticity field responds accordingly, with a response that is the same for each layer (stratification is uniform). It then necessarily follows that the horizontal velocity response to water column squashing or stretching should be uniform in depth.

Finally, a dispersion relationship for the TRW may be obtained. In the quasi-geostrophic framework the horizontal velocities are given by

$$u = -\frac{1}{f_0 \rho_0} \frac{\partial p}{\partial y}$$

$$v = \frac{1}{f_0 \rho_0} \frac{\partial p}{\partial x}.$$

The amplitudes \hat{u} and \hat{v} thus satisfy

$$\hat{u} = -\frac{i l}{f_0 \rho_0} \hat{p} = \frac{l N_0^2 w_0}{\omega f_0 \gamma \sinh(\gamma H_T)} \cosh(\gamma z)$$

$$\hat{v} = \frac{i k}{f_0 \rho_0} \hat{p} = -\frac{k N_0^2 w_0}{\omega f_0 \gamma \sinh(\gamma H_T)} \cosh(\gamma z).$$

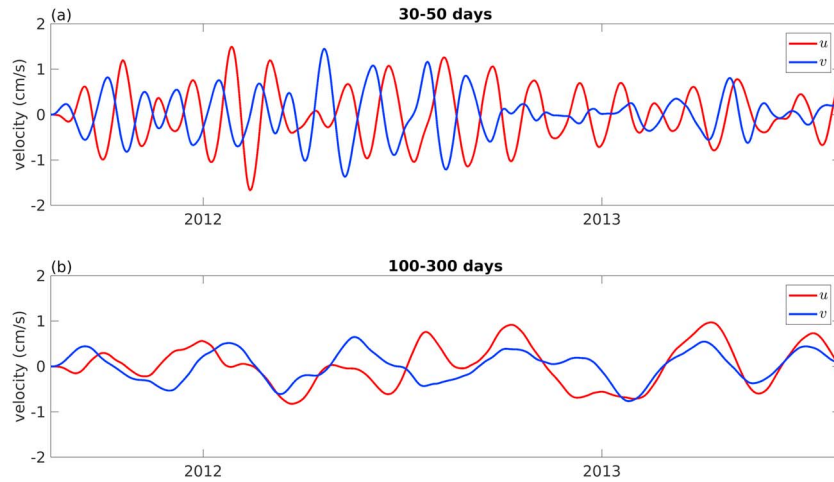


Figure 4. Time series of horizontal velocity (u , red; v , blue) at 2,500-m depth filtered to only retain energy in (a) 30- to 50-day and (b) 100- to 300-day bands. The u and v in the higher-frequency band (panel a) are predominantly out of phase, while they are predominantly in phase with each other in the lower-frequency band (panel b). This rotation of velocity toward the along-isobath direction (northeast-southwest) at lower frequencies is consistent with topographic Rossby wave theory. Note that the 2,500-m depth level is chosen to minimize influences from mesoscale eddies.

The bottom boundary condition requires that $\hat{w} = -\frac{\partial h}{\partial x}\hat{u} - \frac{\partial h}{\partial y}\hat{v}$ at $z = -H_T$. Combining the expressions for \hat{u} , \hat{v} , and \hat{w} yields the dispersion relation

$$\omega = \frac{N_0}{K_H \tanh(\gamma H_T)} \left[k \frac{\partial h}{\partial y} - l \frac{\partial h}{\partial x} \right], \quad \text{with} \quad \gamma = \frac{N_0 K_H}{f_0}.$$

This is consistent with earlier studies of TRWs in a uniform stratification (see, e.g., Meinen et al., 1993). Taking the limit of weak decay ($\gamma H_T \ll 1$) and rotating the coordinate system such that the y axis aligns with the cross-slope direction and the x axis is along-slope yield

$$\omega \approx \frac{f_0}{K_H^2 H_T} k \frac{\partial h}{\partial y^*} = -\frac{\beta^* k}{K_H^2} = -\frac{\beta^* \sin \phi}{K_H}, \quad (10)$$

where $\beta^* = -\frac{f_0}{H_T} \frac{\partial h}{\partial y^*}$ characterizes the topographic β effect and ϕ is the angle between the wave vector and the upslope direction, y^* . This is the TRW analog to the barotropic planetary Rossby wave, where stratification does not show up explicitly. In the vicinity of Mooring D, the slope has a magnitude of $\sim 10^{-3}$. With $f_0 \approx 1.4 \times 10^{-4} \text{ s}^{-1}$ and $H_T \approx 2,500 \text{ m}$, $\beta^* \approx 0.5 \times 10^{-10} \text{ m}^{-1} \text{ s}^{-1}$, comparable in magnitude to planetary β in the midlatitudes.

The dispersion relation shows how the frequency of TRWs depends on wave vector. When the wave vector is predominantly along slope (i.e., $\sin \phi \approx 1$ and water parcel motion is predominantly across slope and the restoring effect of the slope is largest), the waves have a relatively high frequency compared to the case when the wave vector is predominantly across slope (Thompson & Luyten, 1976). This characteristic is clear in the mooring measurements considering the range of subinertial frequencies. Horizontal velocities u and v are out of phase at relatively high frequencies (30–50 days), indicating water parcels preferentially oscillating across slope in the northwest-southeast direction. On the other hand, u and v are mostly in phase at relatively lower frequencies (100–300 days), indicating water parcels preferentially oscillating along slope in the northeast-southwest direction (Figure 4). Ideally, one could filter velocity components into frequency bins to deduce the direction of energy propagation (i.e., the group velocity). However, this is not possible because, in the shallow record, it appears that other velocity sources (possibly eddies) contaminate the wave signal, while the temporal record from the deep MMP is not sufficiently long for such an analysis to be viable. Nevertheless, the evidence presented here (Figure 4) shows consistency with the theory.

5. Summary and Discussion

By examining the depth and frequency distribution of the coherency between moored velocity and potential temperature measurements over a gently sloping bottom in the Canada Basin, we conclude that only vertical

advection can account for the observed subinertial temperature variations. We demonstrate that horizontal and vertical velocities are characterized by different vertical decay length scales, which we show to be consistent with QGPV theory in the limit of weak vertical decay. Important elements of TRW theory, including QGPV theory and cross-slope motions, are shown to be critical in explaining the subinertial deep motions observed in the Beaufort Gyre; TRWs are hence likely sources of the observed subinertial deep motions. The general picture of motions at Mooring D can be summarized as follows. Perturbations that move across the bottom slope cause the water column to stretch/squash. Conservation of potential vorticity then gives rise to the generation of TRWs. These waves propagate with shallow water on the right, passing by Mooring D, yielding the low-frequency signals seen in the u and v measurements. As the water column moves up and down the slope, the concurrent vertical velocity is recorded as subinertial vertical displacements in isopycnals/isotherms. Moreover, the weak, uniform stratification in the deep Canada Basin allows the water column to stretch/squash approximately uniformly, such that the vertical velocity decays linearly upward, which induces a barotropic horizontal velocity.

Two questions naturally arise from the analysis presented here. What is the source of the TRWs? What is the role of TRWs in the energetics and dynamics of the Beaufort Gyre? TRW generation by eddies has been documented in the midlatitudes (e.g., Hamilton, 2009; Oey & Lee, 2002; Pickart, 1995) and may factor in the Beaufort Gyre. The Beaufort Gyre has a ubiquitous mesoscale eddy field, with eddies predominantly located in the halocline (e.g., Zhao & Timmermans, 2015; Zhao et al., 2016), although deeper eddies, centered around the Atlantic Water Layer and deeper have been observed as well (e.g., Bebieva & Timmermans, 2016; Carpenter & Timmermans, 2012). The presence of mesoscale eddies in the halocline dominates the Mooring D record presented here (Figure 2). The coexistence of eddies and TRWs in the measurements is similar to the general situation in the Gulf of Mexico, where the Loop Current and associated eddies dominate the shallow water column and TRWs dominate the deep; modeling studies constrained by observations suggest that these eddies are the source of TRWs in the Gulf of Mexico (e.g., Oey, 2008; Oey & Lee, 2002). An eddy centered in the Canada Basin upper water column can drive flows in the deeper water column when the water column adjusts to the presence of an overlying potential vorticity anomaly (see Zhao & Timmermans, 2015). These flows can excite TRWs at a sloping seafloor (e.g., Hamilton, 2009).

Another source of Beaufort Gyre TRWs may be the barotropic response of the gyre to changes in wind stress (Gill & Niller, 1973; Vinogradova et al., 2007). In the process of geostrophic adjustment, the initial barotropic motions can excite subinertial TRWs that dictate the oceanic adjustment process toward a geostrophically balanced state (Luneva et al., 2012; Yang et al., 2016). Luneva et al. (2012) performed idealized numerical experiments of a homogeneous fluid, initially at rest, and subject to an initial surface perturbation from horizontal, to understand the adjustment process on an f plane. They showed how the flow in a circular basin with a linearly sloping bottom evolves to geostrophic balance via excitation of gravity waves, Kelvin-type waves, and TRWs. For the stratified Beaufort Gyre, the Canada Basin's sloping bottom supports persistent TRWs in response to continually changing surface stresses. Related to wind forcing, we also point out the possibility that wind-driven slope currents at the Canada Basin boundaries may also generate TRWs (see, e.g., Danielson et al., 2014; Peralta-Ferriz et al., 2011).

With respect to Beaufort Gyre energetics, one view of Beaufort Gyre stabilization is that there is a balance between wind-driven Ekman pumping (driving freshwater accumulation in the Beaufort Gyre) and baroclinic instability generating lateral eddy fluxes out of the gyre (releasing freshwater; Manucharyan & Spall, 2016; Meneghello et al., 2017; Yang et al., 2016). That is, an energetic eddy field is responsible for equilibrating the Beaufort Gyre. Alternatively, or in addition, ocean geostrophic currents flowing against the sea ice play a role in regulating spin-up and dissipating energy (see Dewey et al., 2018; Meneghello et al., 2018; Zhong et al., 2018). Persistent TRW activity sheds light on an additional fundamental mechanism for gyre stabilization and energy dissipation. To put the barotropic motions of TRWs within the context of Beaufort Gyre energetics, we compare the eddy kinetic energy (EKE) of columnar motions associated with TRWs against EKE of halocline eddies. Here the depth-integrated EKE is computed as $\int \frac{1}{2}(\overline{u'^2} + \overline{v'^2})dz$, where the overbar denotes time average and u' and v' are horizontal velocity perturbations (i.e., the mean velocity components at each depth are removed from the instantaneous velocity measurements prior to the calculation). Note that the mean flow below the halocline at Mooring D is generally toward the west and $\lesssim 1$ cm/s in magnitude (see Zhao et al., 2018, their Figure 1a), and depth-integrated kinetic energy is dominated by EKE (Zhao et al., 2016, 2018). We separate the eddy-dominated water column shallower than ~ 300 m from the deeper water column dominated by flows likely associated with TRW activity (Figure 2b) and, again, exclude the 2013 segment. The time mean vertically

integrated EKE below the halocline is about $0.3 \text{ m}^3/\text{s}^2$, while the time mean vertically integrated EKE above the halocline is about $0.4 \text{ m}^3/\text{s}^2$. It is thus clear that the near-barotropic motions associated with TRWs contain comparable energy as mesoscale eddies in the upper water column, suggesting that TRWs may be at least as important as mesoscale eddies in dissipating energy (with the understanding that TRWs may be generated by the barotropic response to changes in surface stress or by the eddies themselves).

Results presented here highlight the need for additional long time series velocity measurements in the deep Beaufort Gyre to quantify the role of TRWs. Although the long-duration deep MMP data are limited to Mooring D, there are three other moorings in the set of BGOS moorings (with MMPs measuring the shallow and intermediate water column) spanning the Beaufort Gyre. These show varying levels of kinetic energy (see Zhao et al., 2016, their Figure 3) including an energetic deep eddy field at Mooring B (see Carpenter & Timmermans, 2012). The addition of deep current meter measurements to other BGOS moorings would allow for examination of the local eddy field in conjunction with TRW activity, as well as a basin-scale analysis of TRWs. Deep current measurements made at multiple locations in proximity would allow for wave vector estimates to understand wave pathways. In addition, the source of the waves may be better understood through application of ray tracing theory with knowledge of bottom slope variations and stratification. Further, it will be necessary to examine wind stress curl and sea ice extent in conjunction with deep velocity measurements, including analysis of longer time series to examine whether the TRW field exhibits seasonality. Whether generated from mesoscale eddy activity or barotropic adjustment, or both processes, TRWs are no doubt of key relevance in spin-up, dissipation, and stabilization of the Beaufort Gyre.

Acknowledgments

The mooring data were collected and made available by the Beaufort Gyre Exploration Program based at the Woods Hole Oceanographic Institution (<http://www.whoi.edu/beaufortgyre>) in collaboration with researchers from Fisheries and Oceans Canada at the Institute of Ocean Sciences, with special thanks to Rick Krishfield and Andrey Proshutinsky. We are grateful to two anonymous reviewers and for beneficial discussions associated with the Forum for Arctic Modeling and Observational Synthesis (FAMOS). Funding was provided by the National Science Foundation Division of Polar Programs under award 1350046.

References

- Bebieva, Y., & Timmermans, M.-L. (2016). An examination of double-diffusive processes in a mesoscale eddy in the Arctic Ocean. *Journal of Geophysical Research: Oceans*, 121, 457–475. <https://doi.org/10.1002/2015JC011105>
- Carmack, E. C., Williams, W. J., Zimmermann, S. L., & McLaughlin, F. A. (2012). The Arctic Ocean warms from below. *Geophysical Research Letters*, 39, L07604. <https://doi.org/10.1029/2012GL050890>
- Carpenter, J., & Timmermans, M.-L. (2012). Deep mesoscale eddies in the Canada Basin, Arctic Ocean. *Geophysical Research Letters*, 39, L20602. <https://doi.org/10.1029/2012GL053025>
- Danielson, S. L., Weingartner, T. J., Hedstrom, K. S., Aagaard, K., Woodgate, R., Curchitser, E., & Stabeno, P. J. (2014). Coupled wind-forced controls of the Bering–Chukchi shelf circulation and the Bering Strait throughflow: Ekman transport, continental shelf waves, and variations of the Pacific–Arctic sea surface height gradient. *Progress in Oceanography*, 125, 40–61. <https://doi.org/10.1016/j.pocean.2014.04.006>
- Dewey, S., Morison, J., Kwok, R., Dickinson, S., Morison, D., & Andersen, R. (2018). Arctic ice-ocean coupling and gyre equilibration observed with remote sensing. *Geophysical Research Letters*, 45, 1499–1508. <https://doi.org/10.1002/2017GL076229>
- Dosser, H. V., & Timmermans, M.-L. (2018). Inferring circulation and lateral eddy fluxes in the Arctic Ocean's deep Canada Basin using an inverse method. *Journal of Physical Oceanography*, 48(2), 245–260. <https://doi.org/10.1175/JPO-D-17-0190.1>
- Gill, A., & Niiler, P. (1973). The theory of the seasonal variability in the ocean. *Deep Sea Research and Oceanographic Abstracts*, 20, 141–177.
- Hamilton, P. (2009). Topographic Rossby waves in the Gulf of Mexico. *Progress in Oceanography*, 82(1), 1–31. <https://doi.org/10.1016/j.pocean.2009.04.019>
- Jakobsson, M., Mayer, L., Coakley, B., Dowdeswell, J. A., Forbes, S., Fridman, B., et al. (2012). The International Bathymetric Chart of the Arctic Ocean (IBCAO) version 3.0. *Geophysical Research Letters*, 39, L12609. <https://doi.org/10.1029/2012GL052219>
- Johns, W., & Watts, D. (1986). Time scales and structure of topographic Rossby waves and meanders in the deep Gulf Stream. *Journal of Marine Research*, 44(2), 267–290. <https://doi.org/10.1357/002224086788405356>
- Luneva, M. V., Willmott, A. J., & Maqueda, M. A. M. (2012). Geostrophic adjustment problems in a polar basin. *Atmosphere-Ocean*, 50(2), 134–155. <https://doi.org/10.1080/07055900.2012.659719>
- Manucharyan, G. E., & Spall, M. A. (2016). Wind-driven freshwater buildup and release in the Beaufort Gyre constrained by mesoscale eddies. *Geophysical Research Letters*, 43, 273–282. <https://doi.org/10.1002/2015GL065957>
- Meinen, C., Fields, E., Pickart, R., & Watts, D. (1993). Ray tracing on topographic Rossby waves.
- Meneghello, G., Marshall, J., Cole, S. T., & Timmermans, M.-L. (2017). Observational inferences of lateral eddy diffusivity in the halocline of the Beaufort Gyre. *Geophysical Research Letters*, 44, 12,331–12,338. <https://doi.org/10.1002/2017GL075126>
- Meneghello, G., Marshall, J., Timmermans, M.-L., & Scott, J. (2018). Observations of seasonal upwelling and downwelling in the Beaufort Sea mediated by sea ice. *Journal of Physical Oceanography*, 48(4), 795–805. <https://doi.org/10.1175/JPO-D-17-0188.1>
- Oey, L. (2008). Loop Current and deep eddies. *Journal of Physical Oceanography*, 38(7), 1426–1449. <https://doi.org/10.1175/2007JPO3818.1>
- Oey, L., & Lee, H. (2002). Deep eddy energy and topographic Rossby waves in the Gulf of Mexico. *Journal of physical Oceanography*, 32(12), 3499–3527. [https://doi.org/10.1175/1520-0485\(2002\)032<3499:DEEATR>2.0.CO;2](https://doi.org/10.1175/1520-0485(2002)032<3499:DEEATR>2.0.CO;2)
- Peralta-Ferriz, C., Morison, J. H., Wallace, J. M., & Zhang, J. (2011). A basin-coherent mode of sub-monthly variability in Arctic Ocean bottom pressure. *Geophysical Research Letters*, 38, L14606. <https://doi.org/10.1029/2011GL048142>
- Pickart, R. S. (1995). Gulf Stream—Generated topographic Rossby waves. *Journal of Physical Oceanography*, 25(4), 574–586. [https://doi.org/10.1175/1520-0485\(1995\)025<0574:GSTRW>2.0.CO;2](https://doi.org/10.1175/1520-0485(1995)025<0574:GSTRW>2.0.CO;2)
- Pickart, R. S., & Watts, D. R. (1990). Deep western boundary current variability at Cape Hatteras. *Journal of Marine Research*, 48(4), 765–791. <https://doi.org/10.1357/002224090784988674>
- Proshutinsky, A., Krishfield, R., Timmermans, M.-L., Toole, J., Carmack, E., McLaughlin, F., et al. (2009). Beaufort Gyre freshwater reservoir: State and variability from observations. *Journal of Geophysical Research*, 114, C00A10. <https://doi.org/10.1029/2008JC005104>
- Rhines, P. (1970). Edge-, bottom-, and Rossby waves in a rotating stratified fluid. *Geophysical and Astrophysical Fluid Dynamics*, 1(3-4), 273–302. <https://doi.org/10.1080/03091927009365776>
- Shu, Y., Xue, H., Wang, D., Chai, F., Xie, Q., Cai, S., et al. (2016). Persistent and energetic bottom-trapped topographic Rossby waves observed in the southern South China Sea. *Scientific Reports*, 6, 24338. <https://doi.org/10.1038/srep24338>

- Thompson, R. O., & Luyten, J. R. (1976). Evidence for bottom-trapped topographic Rossby waves from single moorings. *Deep Sea Research And Oceanographic Abstracts* (vol. 23, pp. 629–635). Oxford: Elsevier. [https://doi.org/10.1016/0011-7471\(76\)90005-X](https://doi.org/10.1016/0011-7471(76)90005-X)
- Timmermans, M.-L., & Garrett, C. (2006). Evolution of the deep water in the Canadian Basin in the Arctic Ocean. *Journal of Physical Oceanography*, 36(5), 866–874. <https://doi.org/10.1175/JPO2906.1>
- Timmermans, M.-L., Garrett, C., & Carmack, E. (2003). The thermohaline structure and evolution of the deep waters in the Canada Basin, Arctic Ocean. *Deep Sea Research Part I: Oceanographic Research Papers*, 50(10-11), 1305–1321. [https://doi.org/10.1016/S0967-0637\(03\)00125-0](https://doi.org/10.1016/S0967-0637(03)00125-0)
- Timmermans, M.-L., Melling, H., & Rainville, L. (2007). Dynamics in the deep Canada Basin, Arctic Ocean, inferred by thermistor chain time series. *Journal of Physical Oceanography*, 37(4), 1066–1076. <https://doi.org/10.1175/JPO3032.1>
- Timmermans, M.-L., Rainville, L., Thomas, L., & Proshutinsky, A. (2010). Moored observations of bottom-intensified motions in the deep Canada Basin, Arctic Ocean. *Journal of Marine Research*, 68(3-1), 625–641. <https://doi.org/10.1357/002224010794657137>
- Timmermans, M.-L., Winsor, P., & Whitehead, J. A. (2005). Deep-water flow over the Lomonosov Ridge in the Arctic Ocean. *Journal of Physical Oceanography*, 35(8), 1489–1493. <https://doi.org/10.1175/JPO2765.1>
- Veronis, G. (1981). Dynamic of large-scale ocean circulation. In B. A. Warren & C. Wunsch (Eds.), *Evolution of Physical Oceanography* (pp. 140–183).
- Vinogradova, N. T., Ponte, R. M., & Stammer, D. (2007). Relation between sea level and bottom pressure and the vertical dependence of oceanic variability. *Geophysical research letters*, 34, L03608. <https://doi.org/10.1029/2006GL028588>
- Woodgate, R. A., Aagaard, K., Swift, J. H., Smethie, W. M., & Falkner, K. K. (2007). Atlantic water circulation over the Mendeleev Ridge and Chukchi Borderland from thermohaline intrusions and water mass properties. *Journal of Geophysical Research*, 112, C02005. <https://doi.org/10.1029/2005JC003416>
- Yang, J., Proshutinsky, A., & Lin, X. (2016). Dynamics of an idealized Beaufort Gyre: 1. The effect of a small beta and lack of western boundaries. *Journal of Geophysical Research: Oceans*, 121, 1249–1261. <https://doi.org/10.1002/2015JC011296>
- Zhao, M., & Timmermans, M.-L. (2015). Vertical scales and dynamics of eddies in the Arctic Ocean's Canada Basin. *Journal of Geophysical Research: Oceans*, 120, 8195–8209. <https://doi.org/10.1002/2015JC011251>
- Zhao, M., Timmermans, M.-L., Cole, S., Krishfield, R., & Toole, J. (2016). Evolution of the eddy field in the Arctic Ocean's Canada Basin, 2005–2015. *Geophysical Research Letters*, 43, 8106–8114. <https://doi.org/10.1002/2016GL069671>
- Zhao, M., Timmermans, M.-L., Krishfield, R., & Manucharyan, G. (2018). Partitioning of kinetic energy in the Arctic Ocean's Beaufort Gyre, 123, 4806–4819. <https://doi.org/10.1029/2018JC014037>
- Zhong, W., Steele, M., Zhang, J., & Zhao, J. (2018). Greater role of geostrophic currents in Ekman dynamics in the western Arctic Ocean as a mechanism for Beaufort Gyre stabilization. *Journal of Geophysical Research: Oceans*, 123, 149–165. <https://doi.org/10.1002/2017JC013282>